Original Article

A modified impactor for establishing a graded contusion spinal cord injury model in rats

Rongbao Yan[#], Erliang Li[#], Kang Yan, Qian Zhang, Yanhua Wen, Rui Zhang, Yonghong Wu, Jin Sun, Xin Dong, Qiong Ma, Bo Liao

Department of Orthopedics, Tangdu Hospital, Fourth Military Medical University, Xi'an, China

Contributions: (I) Conception and design: R Yan, E Li; (II) Administrative support: K Yan, X Dong; (III) Provision of study materials or patients: Y Wen, R Zhang; (IV) Collection and assembly of data: Q Zhang, Y Wu; (V) Data analysis and interpretation: J Sun; (VI) Manuscript writing: All authors; (VII) Final approval of manuscript: All authors.

[#]These authors contributed equally to this work.

Correspondence to: Bo Liao; Qiong Ma; Xin Dong. Department of Orthopedics, Tangdu Hospital, Fourth Military Medical University, Xi'an 710000, China. Email: tdyyjzlb@126.com; maqiong@fmmu.edu.cn; dongxin_spine@fmnu.edu.cn.

Background: Given the indispensable role of animal models in preclinical studies of spinal cord injury (SCI) and the current state of available impactors, we designed a modified impactor for establishing contusion SCI in rats. The major improvement is the replacement of the impactor rod with a weight and an impactor tip.

Methods: Preoperatively, radiographs of 8-week-old female Wistar rats were taken to establish a protocol for locating the target spinal segment. A total of 72 rats were randomly divided into 4 groups: the sham, 12.5-, 25- and 50-mm groups. Within 35 days postinjury (dpi), the Basso, Beattie, and Bresnahan locomotor rating scale (BBB) was used to evaluate the hindlimb motor function of the rats. At 7 dpi, the rats were sacrificed, and the spinal cord tissue was fixed. Hematoxylin-eosin (HE) staining was used to assess histological changes. Subsequently, immunofluorescence staining was performed to visualize the expression and distribution of GFAP, CD68, MBP, and NeuN. Additionally, rats were sacrificed, and their tissues were extracted for relevant protein assays. At 3 and 7 dpi, electrophysiological function was evaluated by measuring motor evoked potentials (MEPs) and sensory evoked potentials (SEPs).

Results: The behavioral results revealed that higher strike heights were associated with lower BBB scores. Over time, the BBB scores of the SCI rats exhibited an improving trend. Quantitative analysis of the lesions indicated that as the impact height increased, the area of histological destruction, GFAP-negative area, CD68-positive cell count, and MBP-positive destruction area increased, and the number of NeuN-positive cells decreased. Western blot analysis further verified relevant protein changes. Electrophysiology confirmed that the MEP and SEP amplitudes decreased as the strike height increased.

Conclusions: Thus, these results confirm that this modified impactor can be used to establish a graded SCI model in rats. The model is clinically relevant, reproducible, stable, accessible, and affordable, providing a practical tool with which to elucidate the pathophysiological mechanisms and potential therapies for contusive SCI.

Keywords: Spinal cord injury (SCI); modified impactor; animal model; contusion

Submitted Nov 03, 2021. Accepted for publication Jan 28, 2022.

doi: 10.21037/atm-21-5851

View this article at: https://dx.doi.org/10.21037/atm-21-5851

Introduction

Spinal cord injury (SCI) is a devastating incident that results in loss of motor, sensory, and autonomic nervous system function below the level of injury, causing lasting physical, psychological and occupational damage in the patient. However, there are currently no available curative interventions for SCI (1,2). Animal models play an indispensable role in elucidating the pathophysiology of SCI and studying new therapies preclinically. The rat contusion model is the most commonly used model in SCI research and is similar to the clinical SCI seen in humans (3,4). The contusion SCI model has evolved considerably since Allen established the first weight drop contusion model in 1911 (5). The New York University (NYU)/Multicenter Animal Spinal Cord Injury Studies (MASCIS) impactor, which researchers use to induce SCI to different degrees by dropping a fixed weight on the target level of the spinal cord from different heights, is widely used to generate reproducible and validated contusions in rat models. However, the NYU/MASCIS impactor has inherent deficiencies. The impactor rod may rub against the channel when falling, causing the actual velocity to not reach the desired velocity. The impactor head may be off-center, resulting in inconsistent bilateral injury or even failure of model establishment due to the impactor striking bone. The impactor rod may rebound after landing on the spinal cord surface, resulting in variability. In addition, the duration of contact between the impactor rod and the spinal cord is not precisely controlled (6-9). Thus, precisely controlling the biomechanical instrument to produce reproducible and consistent SCI is challenging.

Considering the possible deficiencies of the NYU/MASCIS impactor mentioned above, we designed a modified impactor to establish an SCI model in rats based on Allen's method (5). This device consists of a stereotaxic frame, a channel with holes, a pulling rod, a weight (10 g), an impactor tip (weight of 0.2 g, diameter of 2.5 mm), vertebral clamps, and an animal platform (*Figure 1A*,*1B*). The main improvement is the replacement of the impactor rod with a weight of concentrated mass and a passive impactor tip of slight mass. Prepositioning the passive impactor tip in the center of the spinal cord surface may reduce the deviation of the drop point. The weight with a lower center of gravity and less friction with the channel may decrease rebound and injury variability. The impactor tip was placed on the dorsal surface of the spinal cord and the spinal cord was then compressed by dropping the weight from different heights to establish a contusion SCI model. In this study, we used a modified impactor to determine whether different degrees of SCI can be established and whether such graded SCI can result in severity-dependent behavioral, histological, and electrophysiological outcomes. We present the following article in accordance with the ARRIVE reporting checklist (available at https://atm.amegroups.com/article/view/10.21037/atm-21-5851/rc).

Methods

Animals

In this experiment, 8-week-old female Wistar rats [SPF Biotechnology Co., Ltd., Beijing, China. certificate no. SCXK (Jing) 2019-0010] weighing approximately 200–230 g were used. The rats were acclimatized for 1 week prior to the experiment. Throughout the study, the rats were given free access to food and water and were housed on a 12-hour light/dark cycle with their littermates in an environmentally controlled room (22–24 ℃). All experimental procedures were approved by the Animal and Ethics Committee of the Experimental Animal Center of Air Force Medical University (No. IACUC-20201003), in compliance with the national guidelines for the care and use of animals.

Contusion SCI model

Random numbers were generated via the standard = RAND () function in Microsoft Excel (version 2019, Microsoft Corp., Redmond, WA, USA). A total of 72 rats were randomly divided into 4 groups: the sham (laminectomy only without SCI), 12.5-mm contusion SCI, 25-mm contusion SCI and 50-mm contusion SCI groups (*Figure 1C*). Only the investigator performing the randomization grouping was aware of the rat allocation, and the rest of the investigators were unaware of this.

The rats were anesthetized by intraperitoneal injection of 3% sodium pentobarbital (40 mg/kg). The dorsal skin was shaved and disinfected with betadine, and a longitudinal incision approximately 2 cm in length was made above the center of the T8-10 spinous processes. The muscles were dissected; the T8, T9, and T10 spinous processes were removed with microsurgical instruments; and the T9 lamina was removed to fully expose the spinal cord. Rats in the sham group were subjected to laminectomy only. A modified impactor was

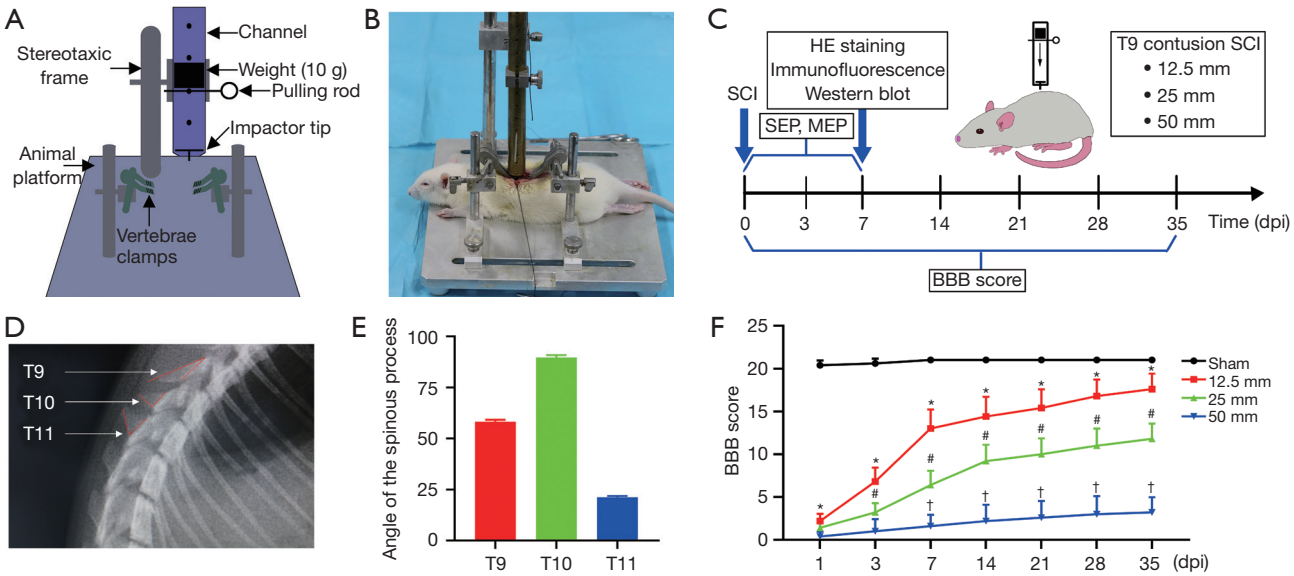

Figure 1 Method for establishing a contusion SCI model, experimental design and behavioral assessment (n=5). (A) Schematic diagram of the impactor. The impactor utilizes tubes with holes to allow weights to be dropped from different heights to induce SCI of different severities. (B) Immobilization of the rat spine using vertebral clamps. The impactor was applied to induce contusion SCI. (C) Schematic of the study design. Contusion SCI models were induced at different heights of impact. MEPs and SEPs were monitored at 3 and 7 dpi. At 7 dpi, the rats were sacrificed and perfused, and their tissues were fixed for HE staining and immunofluorescence analysis. Additionally, rats were sacrificed, and their tissues were extracted for relevant protein assays. Throughout a 35-day period, BBB scores were calculated to evaluate the motor function of the rats. (D) Representative images of lateral X-rays of the rat thoracic spine. The red angles represent the orientation of the T9, T10, and T11 spinous processes. (E) The angle formed by the T9, T10, and T11 spinous processes. (F) Temporal changes in BBB scores after SCI induced by the impactor at different heights. Differences in BBB scores among groups are expressed as follows: *, P<0.05 *vs.* the sham group; #, P<0.05 *vs.* the 12.5-mm group; †, P<0.05 *vs.* the 25-mm group. SCI, spinal cord injury; SEP, sensory evoked potential; MEP, motor evoked potential; HE, hematoxylin-eosin; BBB, Basso, Beattie, and Bresnahan locomotor rating scale.

used to establish a contusion SCI model. The T8 and T10 vertebrae were fixed using vertebral clamps. The stereotaxic frame was adjusted such that the impactor tip was centered on the spinal cord at T9 and tightly attached to its surface, and the height of the weight was adjusted to 12.5, 25, or 50 mm. The pulling rod was pulled out, the weight was dropped from the corresponding height, and the impactor tip impacted the spinal cord for precisely 5 seconds. The tails of the rats twitched spasmodically, and the bilateral hind limbs twitched. Subdural congestion was seen in the impact region after removal of the impactor tip. Eventually, the tissues were sutured layer by layer. Throughout the whole surgery, the body temperature of the rats was maintained at approximately 37 ℃ using a heating pad. All procedures were performed by one experimenter, while the impactor was operated on by another experimenter.

After the surgery, the bladders of the rats were massaged twice daily until urination function was restored. Buprenorphine (0.05 mg/kg) was injected subcutaneously daily for 3 days, and cefazolin (50 mg/kg) was administered subcutaneously once daily for 7 days. From the beginning to the end of the experiment, the general condition of the rats was assessed, and wounds, infections, and other alterations were monitored daily. Animals were excluded if they died prematurely.

X-ray

X-ray imaging was performed to confirm the surgical segments T9, T10, and T11. Briefly, 8-week-old rats were injected intraperitoneally with sodium pentobarbital (40 mg/kg) to prevent movement. Lateral radiographs of the thoracic spine were taken with an X-ray apparatus (Multimobil 2.5, Siemens Healthineers, Forchheim, Germany). The rats were placed on an X-ray collection

plate in the lateral recumbent position 20 cm from the X-ray tube. The X-ray exposure conditions were a voltage of 40 kV, a current of 50 mA and an exposure time of 50 milliseconds. Image analysis was performed using ImageJ software (version 1.52, National Institutes of Health, Bethesda, MD, USA).

The Basso, Beattie, and Bresnahan locomotor rating scale (BBB)

To assess the recovery of hindlimb function in an open field arena after SCI, the BBB scale, which is used to assess several aspects of locomotion, including joint movement, walking ability, trunk stability, limb coordination, tail position and fine movement of the paws, was used to evaluate the rats (10,11). Scores ranged from 21 to 0, which indicated normal movement and complete paralysis, respectively. BBB scores were evaluated at 1, 3, 7, 14, 21, 28, and 35 days postinjury (dpi) by two investigators who were blinded to the groups and adequately trained. If there was inconsistency between the scores assigned by the investigators, a consensus score was determined by discussion.

Hematoxylin-eosin (HE) staining

The rats were deeply anesthetized with pentobarbital (100 mg/kg) at 7 dpi. The thoracic cavity was opened, a blunt needle was inserted into the aorta from the left ventricle, and the right auricle of the heart was cut. The blood was flushed out by perfusion with 300 mL of 0.9% saline, and the tissue was fixed by perfusion of 300 mL of 4% paraformaldehyde. A 5 mm long piece of thoracic spinal cord tissue centered around the lesion was removed, and the tissue was stored at 4 ℃ in 4% paraformaldehyde for 24 hours. The fixed tissues were dehydrated in gradient ethanol solutions, transparentized with x ylene and embedded in paraffin. Serial transverse slices were cut using a microtome at a thickness of 3 μm. Sections centered around the damaged area were selected for analysis.

Briefly, the sections were deparaffinized in xylene, hydrated in gradient ethanol solutions and washed with distilled water. Next, the sections were stained with hematoxylin for 5 minutes and rinsed with distilled water. Then, the sections were incubated in 1% acid ethanol for 10 seconds and rinsed sufficiently. After that, the sections were stained with eosin for 5 minutes and rinsed sufficiently. Next, the sections were dehydrated in gradient ethanol solutions (70%, 80%, 90%, 95%, and 100%) and transparentized with xylene. Finally, the sections were embedded with neutral resin. The slices were observed under an inverted microscope (BX51, Olympus, Tokyo, Japan), and the images were analyzed with ImageJ software.

Immunofluorescence staining

Paraffin-embedded tissue sections were deparaffinized in xylene and hydrated in gradient ethanol solutions. The sections were subjected to antigen repair by incubating them in sodium citrate buffer in a microwave for 10 minutes and then rinsed with 0.1 M phosphate-buffered saline (PBS). The sections were permeabilized with 0.3% Triton X-100 for 10 minutes and then rinsed with PBS. The sections were blocked with 5% goat serum for 1 hour at room temperature, and then incubated with primary antibody overnight at 4 ℃ in a wet box. The following primary antibodies were used: mouse anti-GFAP, clone GA5 (1:100 dilution, Millipore, Temecula, CA, USA), rabbit anti-CD68 (1:200, Abcam, Cambridge, UK), mouse anti-MBP [MBP2] (1:100, Abcam), and rabbit anti-NeuN [EPR12763] (1:200, Abcam). After three rinses in PBS for 10 minutes each, the sections were incubated with Coralite488-conjugated goat anti-rabbit IgG (1:200, Proteintech, Wuhan, China) or Cy3-conjugated goat anti-mouse IgG (1:100, Proteintech) for 1 hour at room temperature. The sections were washed in PBS 3 times and then coverslipped with a drop of anti-fade DAPI-Fluoromount G (SouthernBiotech, Birmingham, AL, USA) for nuclear counterstaining. The sections were visualized with an inverted fluorescence microscope BX51, and the images were analyzed with ImageJ software.

Western blot analysis

Thoracic spinal cord tissues (5 mm) centered around the injury site were collected and frozen in liquid nitrogen at 7 dpi. Total protein was extracted with the Minute total protein extraction kit (Inventbiotech, Plymouth, MN, USA) according to the manufacturer's protocol. The protein concentration was immediately determined by the BCA protein assay kit (Beyotime Biotechnology, Shanghai, China). The protein samples were dissolved in loading buffer and then boiled at 100 ℃ for 5 minutes. Equivalent amounts of protein were loaded in sodium dodecyl sulfate-polyacrylamide gel electrophoresis (SDS-PAGE)

gels for electrophoresis and subsequently transferred to polyvinylidene fluoride (PVDF) membranes (Millipore).

The membranes were blocked with 5% skim milk on a shaker for 2 hours at room temperature. Subsequently, the membranes were incubated with primary antibodies, including mouse anti-GFAP, clone GA5 (1:1,000, Millipore), rabbit anti-CD68 (1:2,000, Abcam), mouse anti-MBP [MBP2] (1:2,000, Abcam), rabbit anti-NeuN [EPR12763] (1:2,000, Abcam), and anti-GAPDH (1:8,000, Abcam), overnight at 4 ℃. After three rinses in Tris-buffered saline with Tween (TBST) for 10 minutes each, the membranes were incubated with horseradish peroxidase-conjugated goat anti-rabbit and mouse IgG (1:4,000, Abmart, Shanghai, China) for 1 hour at room temperature. After being rinsed with TBST (10 minutes, 3 times), the bands were visualized with an electrochemiluminescence (ECL) detection kit (Millipore), and the grayscale values of the protein bands were quantified with ImageJ software.

Electrophysiological evaluation

A multichannel physiological signal recorder (version RM6240E, Chengdu Instrument Factory, Chengdu, China) was used to measure the motor evoked potentials (MEPs) and sensory evoked potentials (SEPs) of rats at 3 and 7 dpi, and baseline recordings were performed prior to laminectomy. All rats were anesthetized by intraperitoneal injection of sodium pentobarbital (40 mg/kg). A hole was made with a dental drill 2 mm posterior to bregma and 3 mm lateral to the midline to expose the right sensorimotor cortex area, and blunt instruments were used to carefully expose the left sciatic nerve. To measure MEPs, stimulating electrodes were placed on the right cortical sensorimotor area, recording electrodes were inserted into the biceps femoris muscle in the left hindlimb, and reference electrodes were positioned subcutaneously on the neck. To measure SEPs, stimulating electrodes were placed on the left sciatic nerve, recording electrodes were placed at the same cortical area as the MEP stimulation electrodes, and reference electrodes were placed in the caudal subcutaneous region.

The MEP and SEP stimulation parameters were as follows: positive current stimulation, intensity =2 mA, frequency =5 Hz, pulse width =0.2 milliseconds, and duration =10 seconds. The software accompanying the RM6240E system was used to record electrophysiological waveform curves, which were subsequently used to calculate amplitudes (mV). The amplitude was defined as the voltage difference from the peak of the first positive peak to the first negative peak.

Statistical analysis

The data are presented as the mean ± standard deviation. SPSS (version 22.0, IBM Corp., Armonk, NY, USA) and GraphPad Prism (version 8.30, GraphPad Prism Inc., San Diego, CA, USA) were used for data analysis and visualization of the results. BBB scores were analyzed using repeated measures two-way analysis of variance (ANOVA) followed by Tukey's post hoc test for multiple comparisons. Histological data, immunofluorescence data, Western blot data, and electrophysiological parameters were compared between multiple groups using one-way ANOVA with Tukey's post hoc comparisons. Correlation analysis between variables was performed using Spearman's rank correlation coefficient. The level of statistical significance was $P<0.05$.

Results

Orientation of the T9, T10, and T11 spinous processes

The triangle formed by the T9, T10, and T11 spinous processes serves as a reliable marker for locating the T9 vertebrae. In particular, the T9 spinous process points caudally, the T10 spinous process points dorsally, and the T11 spinous process points rostrally (*Figure 1D,1E*). X-rays were used to assess the orientation of the spinous processes in 8-week-old rats. The results showed that the angles of the T9, T10 and T11 spinous processes were 58.26±0.87, 89.76±1.03 and 21.13±0.70, respectively.

Behavioral scores

A trend toward gradual recovery of BBB scores was observed in all SCI groups over a 35-day period (*Figure 1F*). All SCI groups exhibited reduced BBB scores compared with the sham-operated group, with statistically significant differences ($P<0.05$). A significant difference in BBB scores was observed between the 25-mm group and the 12.5-mm group at 3 dpi ($P<0.05$), and this difference persisted until the last observation time point. BBB scores were significantly different between the 25-mm group and the 50-mm group at 7 dpi ($P<0.05$), and the difference persisted until 35 dpi. In short, the group with the higher strike height had lower behavioral scores than the other groups at the same time point.

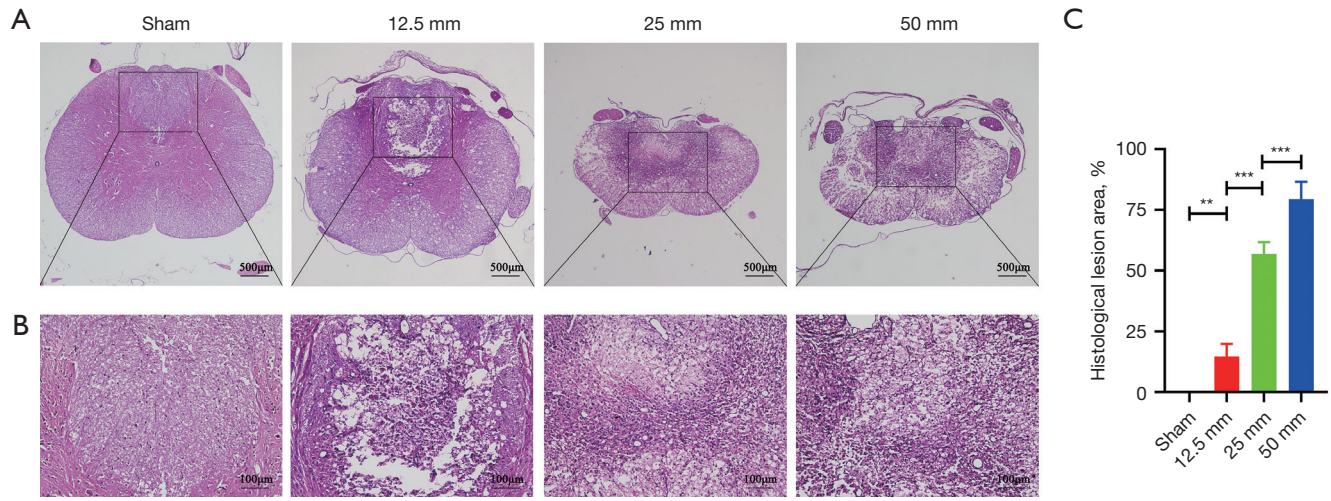

Figure 2 Histological changes in rats after SCI induced by different height strikes (n=4). (A) Representative graphs of HE staining in the sham group, 12.5-, 25-, and 50-mm groups at 7 dpi. Scale bar =500 μm. (B) Representative magnified images of the four groups. Scale bar =100 μm. (C) Comparison of the percentage of lesion area revealed by HE staining in the different groups. **, P<0.01; ***, P<0.001. SCI, spinal cord injury; HE, hematoxylin-eosin.

Histological assessment

At 7 dpi, the rats were sacrificed, and spinal cord tissues were fixed for HE staining (*Figure 2A,2B*). HE staining demonstrated a normal spinal cord structure in the sham group. There was a clear boundary between the gray and white matter, and normal neuronal structures were clearly visible in the gray matter. In the 12.5-mm group, the dorsal spinal cord structures were disrupted, and localized blurring of the boundaries of gray and white matter, tissue swelling, and scattered vacuolar-like changes were observed. In the 25-mm group, the destruction was further expanded, with blurred gray-white matter boundaries and a significant reduction in the number of normal neuronal structures being observed. In the 50-mm group, most of the spinal cord structures were destroyed, there was marked infiltration of inflammatory cells and almost no normal neuronal structures were visible. Furthermore, the percentage of the destroyed spinal cord area relative to the total spinal cord area was quantified, and the results showed that as the height of the impact increased, the more severely the spinal cord tissue was destroyed, and the difference between the groups was statistically significant (*Figure 2C*, P<0.05).

Immunofluorescence evaluation

GFAP and CD68 double immunofluorescence staining revealed the distribution of astrocytes and microglia/macrophages (*Figure 3A*). MBP and NeuN immunofluorescence staining revealed areas of MBP-positive destroyed tissue and the number of NeuN-positive neurons in the spinal cord (*Figure 3B*). Specifically, a small irregularly shaped GFAP-negative region was present in the spinal cord tissues of rats in the 12.5-mm group. The size of this GFAP-negative region increased significantly with increasing strike height. Further analysis revealed a statistically significant difference in the percentage of the GFAP-negative area between the groups with different strike heights (P<0.05), whereas there was no difference between the sham and 12.5-mm groups (*Figure 3C*). Moreover, CD68-positive cell counts suggested that there were different numbers of microglia/macrophages in the different groups. The results showed that the higher the strike height was, the higher the number of CD68-positive cells. The difference was not statistically significant between the sham and 12.5-mm groups only. Interestingly, the merged fluorescence images showed that GFAP-positive cells were lost in the center of the injury site and were replaced by CD68-positive cells (*Figure 3D*).

MBP immunostaining revealed areas of MBP-positive destroyed tissue in the spinal cord. Within the MBP-positive destroyed tissue, MBP-positive structures were disorganized and fragmented, resulting in tissue loss of varying shapes and sizes. As the height of the impact increased, the extent of the disrupted area expanded. The

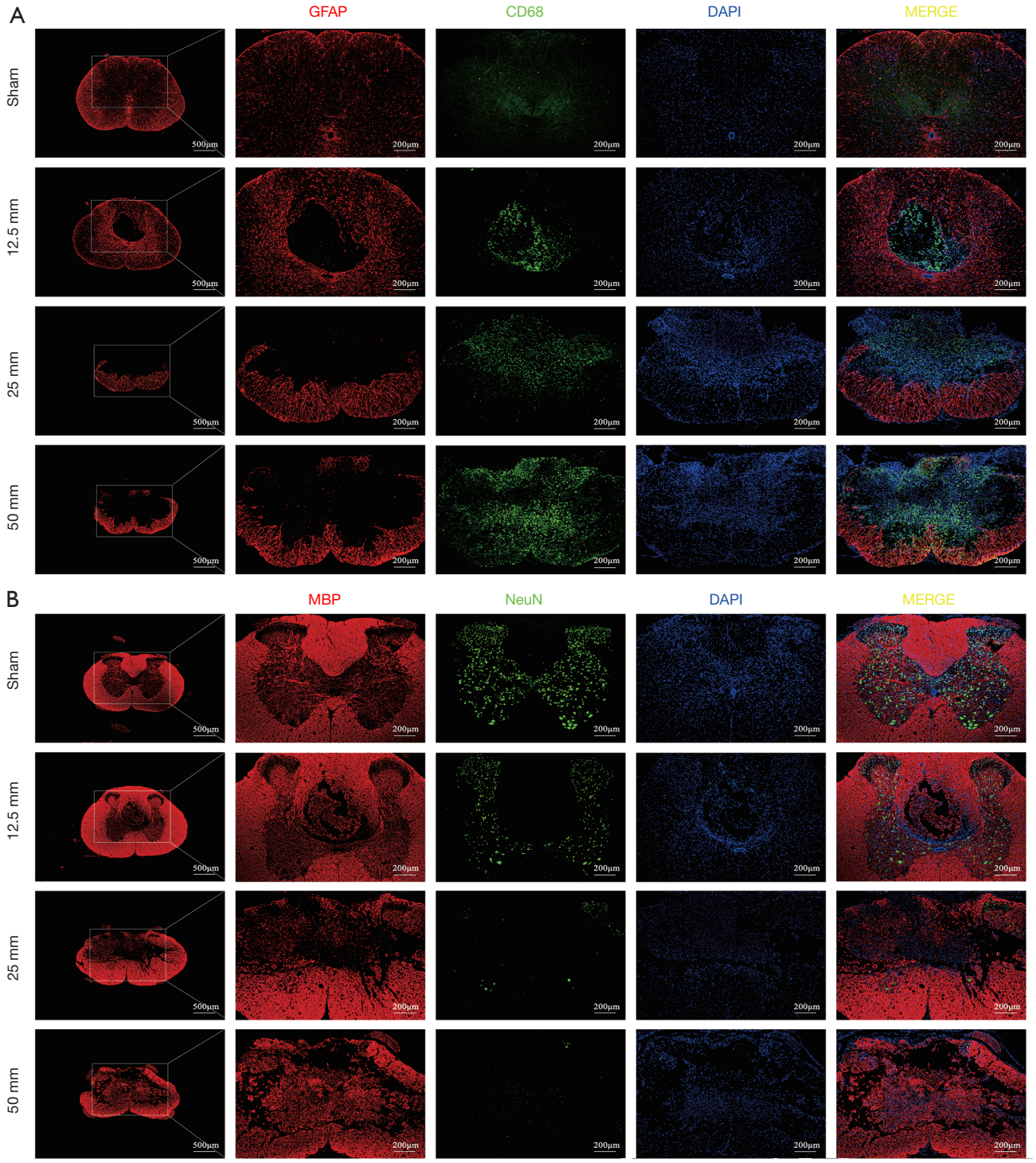

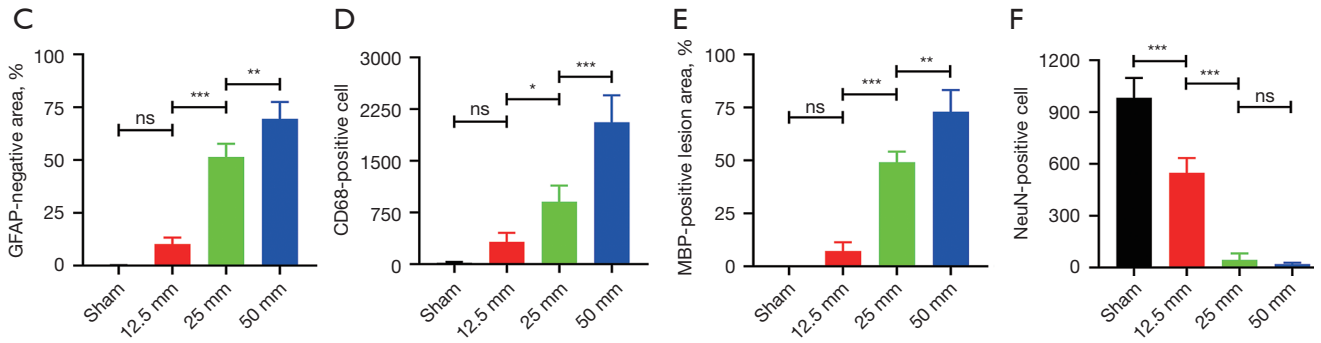

Figure 3 Double immunofluorescence staining for GFAP (red) and CD68 (green) and for MBP (red) and NeuN (green) at 7 dpi (n=4). (A) Representative images of GFAP and CD68 immunofluorescence staining at 7 dpi in the sham-operated group, 12.5-, 25- and 50-mm groups. Scale bar =500 μm in the contour images of spinal cord tissue; scale bar =200 μm in the high magnification image. (B) Representative images of MBP and NeuN immunofluorescence staining in the groups of different strike heights. (C) Intergroup comparison of the percentage of GFAP-negative area. (D) Comparison of CD68-positive cell counts between the four groups. (E) Comparison of the percentage of MBP-positive destruction area in the groups of different strike heights. (F) Intergroup comparison of the number of NeuN-positive cell counts. *, P<0.05; **, P<0.01; ***, P<0.001. ns, not significant.

analysis showed that the percentage of MBP-positive destroyed tissue was significantly different between the groups of different heights (P<0.05) except for the sham and 12.5-mm groups (*Figure 3E*). Furthermore, the number of NeuN-positive neurons in the damaged spinal cord gray matter was counted. Specifically, the number of NeuN-positive cells decreased from 982.50±114.79 in the sham-operated group to 548.00±86.29 in the 12.5-mm group, 45.00±37.05 in the 25-mm group, and 20.25±7.68 in the 50-mm group. The differences between the groups, except for the 25- and 50-mm groups, were significantly different (P<0.05). In addition, there were almost no NeuN-positive neurons in the region of MBP-positive destroyed tissue (*Figure 3F*).

Western blot analysis

To investigate the protein expression of GFAP, CD68, MBP, and NeuN in spinal cord tissue, the rats were sacrificed, and Western blot analysis was performed at 7 dpi (*Figure 4A*). The results showed that the expression of CD68 was lowest in the sham group and that the relative expression of CD68 increased with increasing strike height. The protein expression of GFAP was the highest in the sham group, and the protein expression of GFAP gradually decreased as the strike height increased. The trend in the relative expression of MBP and NeuN was similar to that of GFAP. Comparative expression of GFAP, CD68, MBP, and NeuN protein among the different groups was visualized (*Figure 4B-4E*).

Electrophysiological assessment

MEPs and SEPs were recorded at 3 and 7 dpi, and representative images are shown (*Figure 5A,5B*). The MEP amplitude was the highest in the sham group (593.06±36.97), followed by the 12.5-mm group (466.78±75.36), the 25-mm group (359.06±53.92), and the 50-mm group (295.55±37.11) at 3 dpi. At 7 dpi, the trend in the MEP amplitude was similar between the four groups. Intergroup analysis showed that the differences in amplitude change between the sham and 12.5-mm groups were not statistically significant, while the differences between the other groups were statistically significant (*Figure 5C*, P<0.05).

The SEP amplitude was the highest in the sham group followed by the 12.5-mm group and was lower in the 25-mm group and the lowest in the 50-mm group at 3 and 7 dpi. The difference was not statistically significant between the 12.5- and 25-mm groups only (*Figure 5D*).

Correlations

Furthermore, correlation analysis revealed the association between strike height and the percentage of histological lesion area, BBB scores, immunofluorescence staining, and electrophysiological parameters. Specifically, different strike

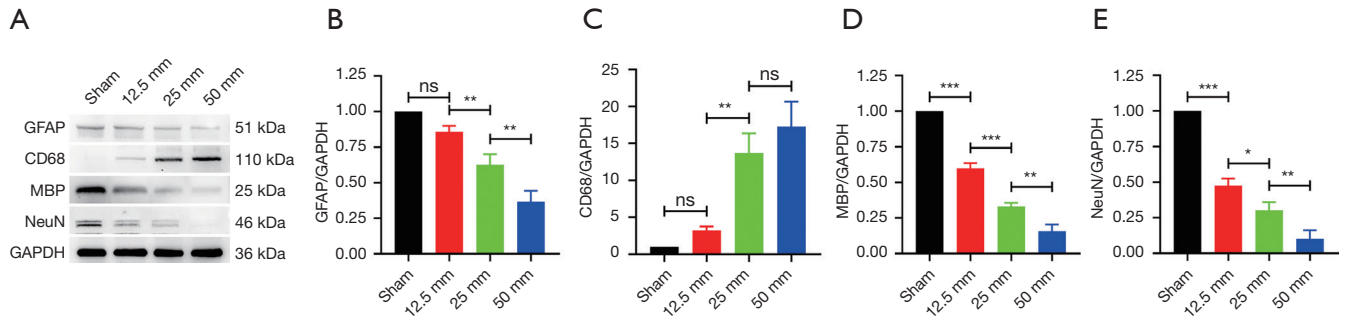

Figure 4 Western blot analysis of the relative expression of GFAP, CD68, MBP, and NeuN in the different groups at 7 dpi (n=4). (A) Western blot bands of GFAP, CD68, MBP, NeuN and the internal reference GAPDH are shown separately. (B-E) Intergroup comparison of the relative expression of GFAP, CD68, MBP, and NeuN in the different groups, with the relative protein expression in the sham group defined as 1. *, P<0.05; **, P<0.01; ***, P<0.001. ns, not significant.

heights were significantly positively and linearly correlated with the percentage of histological injury area (*Figure 6A*). In contrast, negative significant linear correlations were observed between strike height and BBB score at 7, 14, and 21 dpi (*Figure 6B*). Strike height showed a significant positive linear correlation with the GFAP-negative area, CD68-positive cell count, and MBP-positive destruction area but a negative significant correlation with the NeuN cell count (*Figure 6C*). At 3 and 7 dpi, the MEP and SEP amplitudes were also negatively linearly correlated with the strike height (*Figure 6D*).

Discussion

As the most commonly used models in SCI research, rat models have the advantages of being well established and inexpensive; additionally, the injury response in rat models is similar to that observed in humans (12,13). After several revisions by Allen and other researchers, similar weight drop contusion models, including those established with the NYU/MASCIS impactor, have become the most widely used experimental animal model for contusion SCI studies (14,15). Contusion SCI in these models is very similar in nature to human SCI, both of which are caused by the impact of a certain force, resulting in spinal cord edema, ischemia, necrosis, and a series of secondary injury cascades. Furthermore, this established method of SCI maintains the integrity of the dura mater, which effectively prevents the invasion of exogenous components into the SCI area and the leakage of cerebrospinal fluid. In addition, this method allows the selection of specific spinal cord segments and drop heights according to experimental needs.

The improvements of the impactor are as follows. First, the modified impactor uses a passive impactor tip instead of an active impactor rod. The passive impactor tip is placed at the center of the spinal cord surface before striking, which effectively eliminates the deviation of the active impactor rod drop point. The passive impactor tip is lighter in weight (0.2 g), and it does not affect the spinal cord through compression alone. Second, the modified impactor uses a 10 g weight instead of a 10 g impactor rod, reducing the adverse effect caused by the impactor rod rubbing against the channel. The weight strikes the passive impactor tip, which can increase the speed of the impact and reduce the variation in damage severity. Third, the weight has a lower center of gravity than the impactor rod, and the vertebral clamps stabilize the adjacent upper and lower vertebrae, making the impactor tip less likely to rebound when it hits the spinal cord surface. Finally, the materials used for the modified impactor are easily available, the production process is relatively simple, and the cost-benefit ratio is high, making it convenient for general laboratories to use and fabricate the impactor. Based on the above advantages, we used the modified impactor to produce a contusion SCI model in rats.

After being anesthetized, the rats were placed in the supine position on the surgical table, and the high protrusion in the thoracic dorsal spine region was located by touch. We carefully exposed the spinous processes of the thoracic spine and interestingly found that the T9, T10 and T11 spinous processes formed a triangle-like shape. Specifically, the T9 spinous process pointed caudally, the T10 spinous process pointed dorsally, and the T11 spinous process pointed rostrally. Furthermore, we verified this

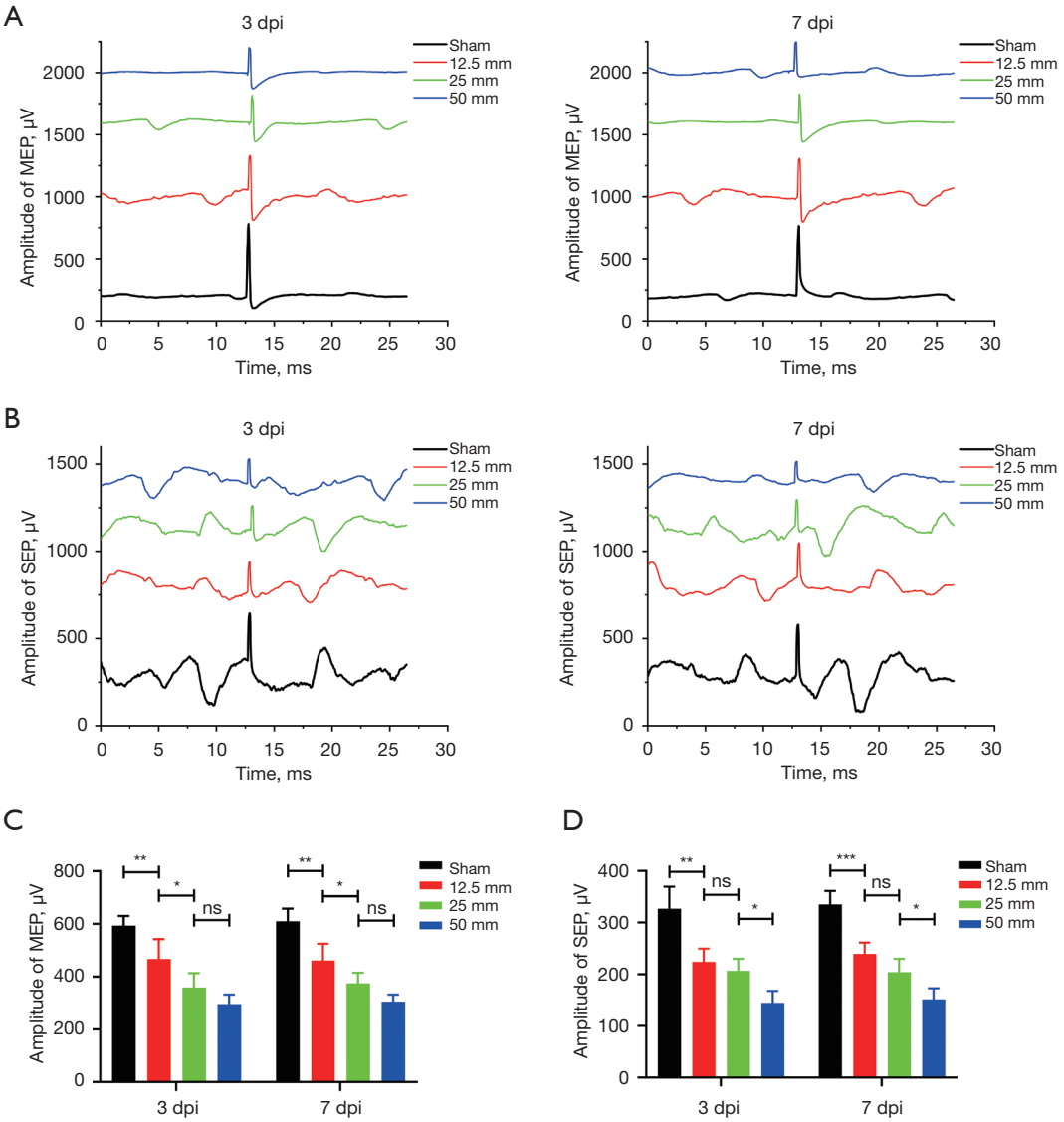

Figure 5 Electrophysiological variations in MEPs and SEPs at 3 and 7 dpi (n=5). (A) Representative MEP waveforms at 3 and 7 dpi in the sham, 12.5-, 25-, and 50-mm groups. (B) Representative SEP waveforms at 3 and 7 dpi in the four groups. (C) Quantitative analysis of the trend in MEP amplitude at 3 and 7 dpi. (D) Quantitative analysis of the trend in SEP amplitude at 3 and 7 dpi. *, P<0.05; **, P<0.01; ***, P<0.001. MEP, motor evoked potential; SEP, sensory evoked potential; ns, not significant.

triangular orientation by obtaining X-rays and measuring the angles of the three spinous processes in 8-week-old rats. We used this triangle at T9-11 to develop a reliable landmark protocol: first, the high prominence of the thoracic dorsum of the rat was identified by touch, and then the T9, T10 and T11 spinous processes were then carefully exposed to reveal their triangular orientation, which allowed the experimenter to accurately locate the target spinal cord region. Thus, we concluded that the contusion SCI model was established in rats at the correct segment.

Based on previous studies (16,17), we used a weight of 10 g and strike heights of 12.5, 25, and 50 mm, which can be used to establish contusion SCI models of different severities in rats. Assessment of locomotor function after SCI is a fundamental method for determining the extent of SCI and assessing spinal cord repair and regeneration. The BBB scale has become the most widely used method for behavioral evaluation after SCI (18,19). In our study,

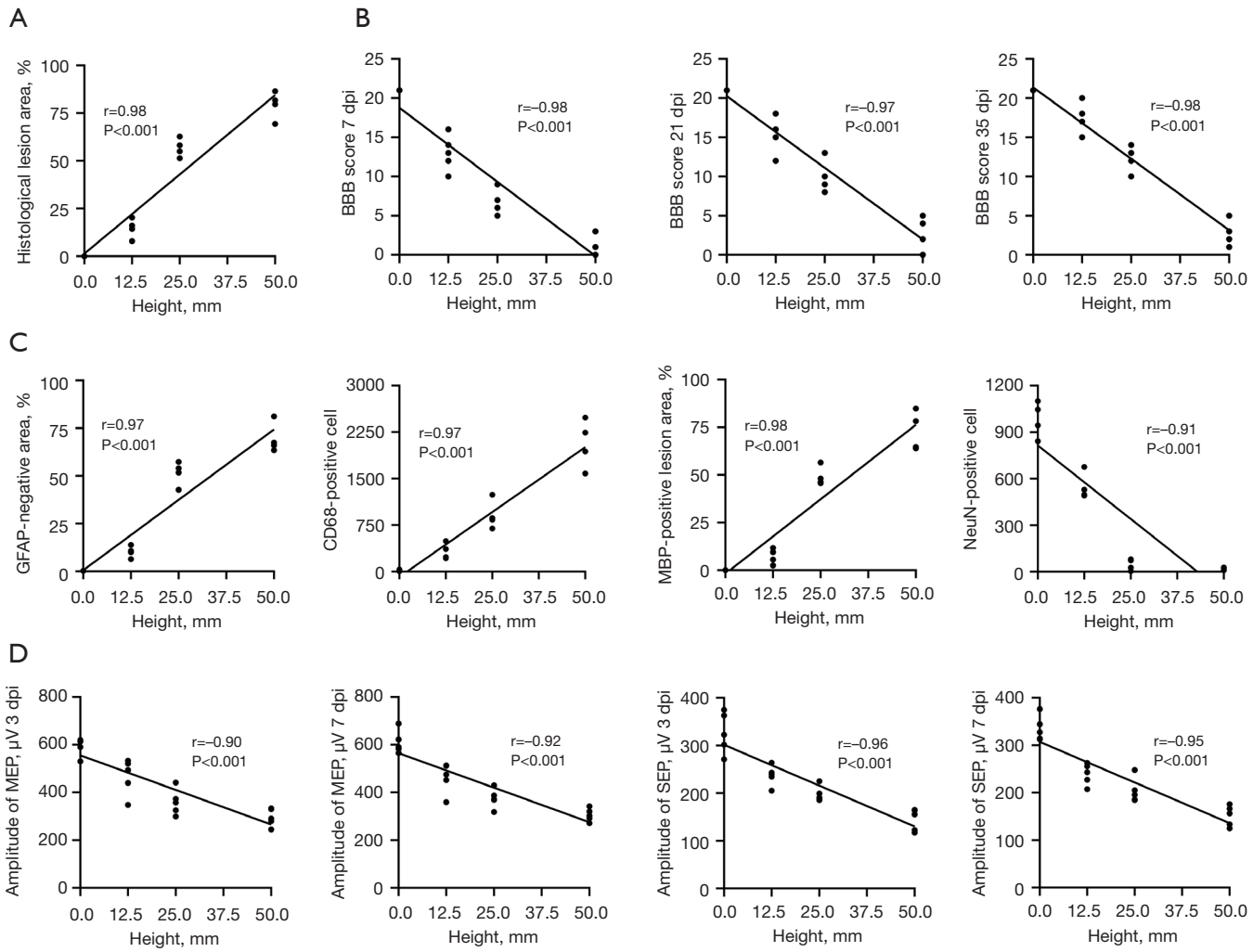

Figure 6 Correlation analysis of strike height with the histological injury area, BBB scores, immunofluorescence staining, and electrophysiological parameters. (A) Correlation of strike height with the percentage of histological injury area. (B) Correlation of strike height with BBB scores at 7, 21, and 35 dpi. (C) Correlation of strike height with the GFAP-negative area, CD68-positive cell count, MBP-positive injured tissue area, and NeuN-positive cell count. (D) Correlation of the strike height with MEP and SEP amplitudes at 3 and 7 dpi. BBB, Basso, Beattie, and Bresnahan locomotor rating scale; MEP, motor evoked potential; SEP, sensory evoked potential.

the hindlimb motor function of rats after SCI was evaluated by BBB scores, which were similar to those in previous studies (20,21). Our results showed that BBB scores were significantly lower in the groups with different strike heights than in the sham-operated group after modeling ($P<0.05$), suggesting that the modified impactor can successfully establish SCI models in rats. The BBB score decreased as the strike height increased, suggesting an increase in SCI severity. These results confirm that the graded SCI model established by the modified impactor produced severity-dependent behavioral outcomes.

The overall morphological structure and cellular changes between the SCI group and the sham-operated group were observed by HE staining. Histological analysis indicated that the greater the height of the impact, the more severe the degree of SCI and the greater the scope of damage to spinal cord structures, which is consistent with previous studies (22,23). Histological analysis provides a complementary explanation of the behavioral outcomes, confirming the differential characteristics of spinal cord tissue damage of different degrees caused by impact from different heights.

Following SCI, astrocytes are activated and produce various chemokines, cytokines, and growth factors that initially exert neuroprotective effects (24,25). GFAP is an intermediate filament protein that is mainly responsible for the proper assembly and development of the astroglial cytoskeleton, which is present in the astrocyte matrix (26). Increased expression of GFAP indicates proliferation and activation of astrocytes in the region of injury. At 1–2 weeks after SCI, reactive astrocytes accumulate at the edge of the lesion and play an active role in blocking the expansion of the injured area. Studies have confirmed that early removal of the astrocyte scar increases the size of the lesion area and reduces functional recovery in mice (27,28). Our study showed that the size of the GFAP-negative region was roughly associated with the severity of SCI at 7 days. Specifically, the higher the strike height is, the larger the GFAP-negative area.

The inflammatory response plays a crucial role in secondary injury after SCI. In response to injury, resident microglia/macrophages are rapidly mobilized to the site of injury and initiate the inflammatory response (29). Microglia/macrophages are activated and release chemokines, cytokines and other inflammatory mediators that recruit neutrophils and macrophages from the peripheral blood into the injured region of the spinal cord (30,31). Microglia/macrophages exacerbate inflammatory injury in the microenvironment by releasing protein hydrolases, reactive oxygen species and inflammatory factors and perform protective functions by removing cellular debris, remodeling cells and producing pro-regenerative factors (32). We selected CD68 as a phenotypic marker of activated microglia/macrophages (33). The results showed that the number of microglia/macrophage-positive cells at 7 dpi increased as the strike height increased, implying that the more severe the damage, the more intense the inflammatory response. Interestingly, we found that GFAP-positive cells in the center of the lesion were lost and were replaced by CD68-positive microglia/macrophages.

In the central nervous system, mature oligodendrocytes interact with neuronal axons in a complex manner to form myelin sheaths, which wrap around the axons of neurons to provide insulation and enable rapid saltatory nerve impulse conduction (34,35). MBP is synthesized and secreted by oligodendrocytes, which play a crucial role in regulating the morphology and stability of myelin structures (36). Previous studies have revealed that mature oligodendrocytes are susceptible to damage after SCI, resulting in disintegration of the axonal skeleton and rupture of the myelin sheath and leading to axonal Wallerian degeneration and release of myelin debris. The accumulation of myelin debris further aggravates the apoptosis of oligodendrocytes and neurons (37,38). Our study showed that MBP-positive injured areas formed in the injury center at 7 dpi. As the strike height increased, the MBP-positive destruction area increased.

After SCI, damage to neurons includes direct neuronal damage from the initial mechanical impact, as well as further neuronal damage from the detrimental neurochemical cascade of secondary injury (39,40). NeuN is a reliable marker protein for mature neurons that can be stably expressed in postmitotic neurons (41). We counted NeuN-positive cells to quantify the total number of neurons and found that the number of NeuN-positive cells decreased with increasing strike height. We also found that NeuN-positive cells were extremely rare within the area of MBP-positive injury.

Evoked potentials can be used to assess the structural and functional status of superior and inferior conduction fibers from the peripheral nerves to the cerebral hemispheres, which indirectly reflect motor and sensory function in rats after SCI (42). After SCI, MEPs can be used to objectively measure the functional integrity of the descending motor pathways in the spinal cord. Similarly, SEPs can be used to assess the functional integrity of the ascending sensory pathway (43). Previous studies have shown that SEP and MEP amplitudes decrease with increasing injury severity (44,45). Our findings are consistent with the abovementioned studies, which revealed that the SEP and MEP amplitudes showed a gradual decrease with increasing injury severity at 3 and 7 dpi.

There are some limitations of this study. One limitation is that BBB scores were used as the only measure of motor function recovery. BBB scores are subjective, and inflammation, the incision, and pain may affect the accuracy of functional recovery assessment in the early stages of SCI (46). In addition, the duration of the strike from the beginning to the end cannot be precisely controlled. Spinal cord impact begins when the pulling rod is manually pulled out and ends when the channel is manually lifted, and this process is kept within 5 seconds as much as possible. Furthermore, it is necessary to control the contact time by digital devices. Moreover, parameters of strike force, velocity, and cord displacement during injury were not identified. Accurate measurement of these injury parameters facilitates the discrimination of variability among multiple individuals, thus improving the consistency and reproducibility of the SCI model in rats.

The determination of injury parameters can be achieved via relevant sensors, which is a future direction of our research. Finally, this experiment was performed only in Wistar rats, and validation of this impactor in other rat strains and mice is pending.

Conclusions

In summary, we designed a modified impactor for establishing a contusion SCI model in rats. Our improvement is primarily in replacing the impactor rod with a mass-concentrated weight and a passive impactor tip of slight mass. Seemingly small improvements will be beneficial, which facilitates the establishment of more accurate SCI models. We have demonstrated that graded SCI can be established using this impactor with strike heights of 12.5, 25, and 50 mm. The model is clinically relevant, reproducible, stable, accessible, and affordable. The results of this study suggest that this impactor is an attractive and viable alternative for further preclinical and clinical studies of SCI.

Acknowledgments

Funding: This work was supported by the National Natural Science Foundation of China (No. 82174166).

Footnote

Reporting Checklist: The authors have completed the ARRIVE reporting checklist. Available at https://atm.amegroups.com/article/view/10.21037/atm-21-5851/rc

Data Sharing Statement: Available at https://atm.amegroups.com/article/view/10.21037/atm-21-5851/dss

Peer Review File: Available at https://atm.amegroups.com/article/view/10.21037/atm-21-5851/prf

Conflicts of Interest: All authors have completed the ICMJE uniform disclosure form (available at https://atm.amegroups.com/article/view/10.21037/atm-21-5851/coif). The authors have no conflicts of interest to declare.

Ethical Statement: The authors are accountable for all aspects of the work in ensuring that questions related to the accuracy or integrity of any part of the work are appropriately investigated and resolved. All experimental procedures were approved by Animal and Ethics Committee of the Experimental Animal Center of the Air Force Medical University (No. IACUC-20201003), in compliance with the national guidelines for the care and use of animals.

References

1. Ahuja CS, Nori S, Tetreault L, et al. Traumatic Spinal Cord Injury-Repair and Regeneration. Neurosurgery 2017;80:S9-22.
2. Badhiwala JH, Ahuja CS, Fehlings MG. Time is spine: a review of translational advances in spinal cord injury. J Neurosurg Spine 2018;30:1-18.
3. Sharif-Alhoseini M, Khormali M, Rezaei M, et al. Animal models of spinal cord injury: a systematic review. Spinal Cord 2017;55:714-21.
4. Kjell J, Olson L. Rat models of spinal cord injury: from pathology to potential therapies. Dis Model Mech 2016;9:1125-37.
5. Allen AR. Surgery of experimental lesion of spinal equivalent to crush injury of fracture dislocation. JAMA 1911;LVII:878.
6. Cheriyan T, Ryan DJ, Weinreb JH, et al. Spinal cord injury models: a review. Spinal Cord 2014;52:588-95.
7. Wu X, Zhang YP, Qu W, et al. A Tissue Displacement-based Contusive Spinal Cord Injury Model in Mice. J Vis Exp 2017;(124):54988.
8. Wu X, Qu W, Bakare AA, et al. A Laser-Guided Spinal Cord Displacement Injury in Adult Mice. J Neurotrauma 2019;36:460-8.
9. Zhang YP, Burke DA, Shields LB, et al. Spinal cord contusion based on precise vertebral stabilization and tissue displacement measured by combined assessment to discriminate small functional differences. J Neurotrauma 2008;25:1227-40.
10. Basso DM, Beattie MS, Bresnahan JC. A sensitive and reliable locomotor rating scale for open field testing in rats. J Neurotrauma 1995;12:1-21.

11. Barros Filho TE, Molina AE. Analysis of the sensitivity and reproducibility of the Basso, Beattie, Bresnahan (BBB) scale in Wistar rats. Clinics (Sao Paulo) 2008;63:103-8.
12. Ahuja CS, Wilson JR, Nori S, et al. Traumatic spinal cord injury. Nat Rev Dis Primers 2017;3:17018.
13. Duan H, Pang Y, Zhao C, et al. A novel, minimally invasive technique to establish the animal model of spinal cord injury. Ann Transl Med 2021;9:881.
14. Zhang N, Fang M, Chen H, et al. Evaluation of spinal cord injury animal models. Neural Regen Res 2014;9:2008-12.
15. Filipp ME, Travis BJ, Henry SS, et al. Differences in neuroplasticity after spinal cord injury in varying animal models and humans. Neural Regen Res 2019;14:7-19.
16. Motovylyak A, Skinner NP, Schmit BD, et al. Longitudinal In Vivo Diffusion Magnetic Resonance Imaging Remote from the Lesion Site in Rat Spinal Cord Injury. J Neurotrauma 2019;36:1389-98.
17. Jirjis MB, Vedantam A, Budde MD, et al. Severity of spinal cord injury influences diffusion tensor imaging of the brain. J Magn Reson Imaging 2016;43:63-74.
18. Scheff SW, Saucier DA, Cain ME. A statistical method for analyzing rating scale data: the BBB locomotor score. J Neurotrauma 2002;19:1251-60.
19. Fouad K, Ng C, Basso DM. Behavioral testing in animal models of spinal cord injury. Exp Neurol 2020;333:113410.
20. Tang Y, Liu HL, Min LX, et al. Serum and cerebrospinal fluid tau protein level as biomarkers for evaluating acute spinal cord injury severity and motor function outcome. Neural Regen Res 2019;14:896-902.
21. Jirjis MB, Kurpad SN, Schmit BD. Ex vivo diffusion tensor imaging of spinal cord injury in rats of varying degrees of severity. J Neurotrauma 2013;30:1577-86.
22. Reynolds JA, Henwood MK, Turtle JD, et al. Brain-Dependent Processes Fuel Pain-Induced Hemorrhage After Spinal Cord Injury. Front Syst Neurosci 2019;13:44.
23. Fedorova J, Kellerova E, Bimbova K, et al. The Histopathology of Severe Graded Compression in Lower Thoracic Spinal Cord Segment of Rat, Evaluated at Late Post-injury Phase. Cell Mol Neurobiol 2022;42:173-93.
24. Gaudet AD, Fonken LK. Glial Cells Shape Pathology and Repair After Spinal Cord Injury. Neurotherapeutics 2018;15:554-77.
25. Faulkner JR, Herrmann JE, Woo MJ, et al. Reactive astrocytes protect tissue and preserve function after spinal cord injury. J Neurosci 2004;24:2143-55.
26. Yeh JZ, Wang DH, Cherng JH, et al. A Collagen-Based Scaffold for Promoting Neural Plasticity in a Rat Model of Spinal Cord Injury. Polymers (Basel) 2020;12:2245.
27. Anderson MA, Burda JE, Ren Y, et al. Astrocyte scar formation aids central nervous system axon regeneration. Nature 2016;532:195-200.
28. Hart CG, Karimi-Abdolrezaee S. Recent insights on astrocyte mechanisms in CNS homeostasis, pathology, and repair. J Neurosci Res 2021;99:2427-62.
29. Yang SS, Lin L, Liu Y, et al. High Morphologic Plasticity of Microglia/Macrophages Following Experimental Intracerebral Hemorrhage in Rats. Int J Mol Sci 2016;17:1181.
30. Bloom O, Herman PE, Spungen AM. Systemic inflammation in traumatic spinal cord injury. Exp Neurol 2020;325:113143.
31. Orr MB, Gensel JC. Spinal Cord Injury Scarring and Inflammation: Therapies Targeting Glial and Inflammatory Responses. Neurotherapeutics 2018;15:541-53.
32. Gensel JC, Zhang B. Macrophage activation and its role in repair and pathology after spinal cord injury. Brain Res 2015;1619:1-11.
33. Chistiakov DA, Killingsworth MC, Myasoedova VA, et al. CD68/macrosialin: not just a histochemical marker. Lab Invest 2017;97:4-13.
34. Domingues HS, Cruz A, Chan JR, et al. Mechanical plasticity during oligodendrocyte differentiation and myelination. Glia 2018;66:5-14.
35. Yan Z, Chu L, Jia X, et al. Myelin basic protein enhances axonal regeneration from neural progenitor cells. Cell Biosci 2021;11:80.
36. Lakshman N, Bourget C, Siu R, et al. Niche-dependent inhibition of neural stem cell proliferation and oligodendrogenesis is mediated by the presence of myelin basic protein. Stem Cells 2021;39:776-86.
37. Pukos N, Goodus MT, Sahinkaya FR, et al. Myelin status and oligodendrocyte lineage cells over time after spinal cord injury: What do we know and what still needs to be unwrapped? Glia 2019;67:2178-202.
38. Chalfouh C, Guillou C, Hardouin J, et al. The Regenerative Effect of Trans-spinal Magnetic Stimulation After Spinal Cord Injury: Mechanisms and Pathways Underlying the Effect. Neurotherapeutics 2020;17:2069-88.
39. Anjum A, Yazid MD, Fauzi Daud M, et al. Spinal Cord Injury: Pathophysiology, Multimolecular Interactions, and Underlying Recovery Mechanisms. Int J Mol Sci 2020;21:7533.
40. Rodríguez-Barrera R, Rivas-González M, García-Sánchez J, et al. Neurogenesis after Spinal Cord Injury: State of the

Art. Cells 2021;10:1499.
41. Duan W, Zhang YP, Hou Z, et al. Novel Insights into NeuN: from Neuronal Marker to Splicing Regulator. Mol Neurobiol 2016;53:1637-47.
42. Li R, Huang ZC, Cui HY, et al. Utility of somatosensory and motor-evoked potentials in reflecting gross and fine motor functions after unilateral cervical spinal cord contusion injury. Neural Regen Res 2021;16:1323-30.
43. Bazley FA, Hu C, Maybhate A, et al. Electrophysiological evaluation of sensory and motor pathways after incomplete unilateral spinal cord contusion. J Neurosurg Spine 2012;16:414-23.
44. Agrawal G, Kerr C, Thakor NV, et al. Characterization of graded multicenter animal spinal cord injury study contusion spinal cord injury using somatosensory-evoked potentials. Spine (Phila Pa 1976) 2010;35:1122-7.
45. Redondo-Castro E, Navarro X, García-Alías G. Longitudinal Evaluation of Residual Cortical and Subcortical Motor Evoked Potentials in Spinal Cord Injured Rats. J Neurotrauma 2016;33:907-16.
46. Agrawal G, Thakor NV, All AH. Evoked potential versus behavior to detect minor insult to the spinal cord in a rat model. J Clin Neurosci 2009;16:1052-5.

Cite this article as: Yan R, Li E, Yan K, Zhang Q, Wen Y, Zhang R, Wu Y, Sun J, Dong X, Ma Q, Liao B. A modified impactor for establishing a graded contusion spinal cord injury model in rats. Ann Transl Med 2022;10(8):436. doi: 10.21037/atm-21-5851